PNAS RESEARCH ARTICLE | CHEMISTRY

Synthesis and characterization of Craig-type antiaromatic species with [4*n* + 2] π electrons

Lina Chen[a,1], Lu Lin[a,b,1], Amit Ranjan Nath[c,1], Qin Zhu[a,1], Zhixin Chen[a], Jingjing Wu[a,b], Hongjian Wang[a], Qian Li[a], Wen-Feng Lin[d], Jun Zhu[a,b,2], and Haiping Xia[a,c,2]

Edited by Kendall Houk, University of California Los Angeles, Los Angeles, CA; received September 18, 2022; accepted December 9, 2022

Antiaromaticity is extended from aromaticity as a complement to describe the unsaturated cyclic molecules with antiaromatic destabilization. To prepare antiaromatic species is a particularly challenging goal in synthetic chemistry because of the thermodynamic instability of such molecules. Among that, both Hückel and Möbius antiaromatic species have been reported, whereas the Craig one has not been realized to date. Here, we report the first example of planar Craig antiaromatic species. Eight Craig antiaromatic compounds were synthesized by deprotonation-induced reduction process and were fully characterized as follows. Single-crystal X-ray crystallography showed that these complexes have planar structures composed of fused five-membered rings with clearly alternating carbon–carbon bond lengths. In addition, proton NMR (^{1}H NMR) spectroscopy in these structures showed distinctive upfield shifts of the proton peaks to the range of antiaromatic peripheral hydrogens. Experimental spectroscopy observations, along with density-functional theory (DFT) calculations, provided evidence for the Craig antiaromaticity of these complexes. Further study experimentally and theoretically revealed that the strong exothermicity of the acid-base neutralization process was the driving force for this challenging transformation forming Craig antiaromatic species. Our findings complete a full cycle of aromatic chemistry, opening an avenue for the development of new class of antiaromatic systems.

aromaticity | Craig-type antiaromaticity | deprotonation-induced reduction process | driving force of aromaticity transformation

Significance

Antiaromaticity is associated with extra thermodynamic instability and makes the synthesis and isolation of antiaromatic molecules particularly challenging. Craig-type (anti)aromaticity, with a reversal to Hückel rule, describes a planar molecule with π-conjugated systems involving p_π–d_π interaction. To synthesize Craig antiaromatic compound is challengeable as it contains a set of properties that initially seems mutually incompatible: 1) antiaromaticity destabilization; 2) a planar structure with [4*n* + 2] π electrons; and 3) p_π–d_π interaction with phase shift in *d* orbital. In this work, we report the first synthesis of the Craig-type antiaromatic compounds via the deprotonation-induced reduction process and the Craig antiaromaticity along with the driving force of realization of Craig-type antiaromatic compounds was evidenced both experimentally and theoretically.

Aromaticity is a fundamental concept in chemistry that was initially proposed to describe electronic delocalization with anomalous stability in π-conjugated molecules; three patterns of ground state aromaticity have since described Hückel (1), Craig (2) and Möbius aromaticity (3) (Fig. 1*A*), and all have been studied both experimentally and theoretically (4–12). The Hückel aromaticity, proposed in 1931, applies to planar molecule with [4*n* + 2] π electrons and has been exemplified by two well-known aromatic molecules, naphthalene (13) and benzene (14) (Fig. 1*B*) that were discovered in the 1820s. In contrast, Craig and Möbius aromaticity, predicted later in 1958 and 1964, respectively, describe molecules with [4*n*] π electrons in π-conjugated systems with a 180° phase shift. Möbius aromaticity is achieved by a 180° (π) half-twist of the *p*-atomic orbitals in conjugated systems into a Möbius strip conformation and the first Möbius aromatic compound [16] annulene was experimentally isolated in 2003 (4). Whereas Craig aromaticity is achieved by introducing the *d*-atomic orbital for 180° phase shift with the p_π–d_π delocalization to retain a planar structure and the first Craig aromatic compound, namely metallapentalyne, was synthesized in 2013 (Fig. 1*B*) (15).

Antiaromaticity was proposed subsequently by Breslow (16) as a complement of aromaticity to describe the π-conjugated molecules with opposite electron counting rule and antiaromatic destabilization, which has not been studied as thoroughly as aromaticity as it is associated a cyclic molecule with high thermodynamic instability (16, 17). Thus, the synthesis of such molecules is particularly challenging, and only a few antiaromatic molecules have been reported thus far (18–23). For instance, the classic Hückel antiaromatic cyclobutadiene was attributed to the synthesis of sterically protected cyclobutadienes by Krebs et al. and Maier et al. in the 1970s (18, 19), and its antiaromaticity was subsequently experimentally characterized in 1999 by Snyder et al. (21). The first Möbius antiaromatic compound Pd-vacataporphyrin was synthesized without attaining a crystal structure in 2008 by Latos-Grażyński et al. (22) (Fig. 1*C*). As for Craig antiaromatic species (2), it was expected to have a planar structure with [4*n* + 2] π electrons, but such geometric and electronic structure is highly likely to exhibit Hückel aromaticity rather than Craig antiaromaticity due to the former endows molecule with extra stability but the latter endows instability. Apart from that, Craig antiaromatic species required an additional *d*-atomic orbital for 180° phase shift with the p_π–d_π interaction. Therefore, the realization of Craig

Author contributions: J.Z. and H.X. designed research; L.C., L.L., A.R.N., Q.Z., Z.C., J.W., H.W., and Q.L. performed research; L.C., L.L., A.R.N., and Q.Z. contributed new reagents/analytic tools; L.C., L.L., Z.C., and J.W. analyzed data; and L.C., W.-F.L., J.Z., and H.X. wrote the paper.

The authors declare no competing interest.

This article is a PNAS Direct Submission.

[1]L.C., L.L., A.R.N. and Q.Z. contributed equally to this work.

[2]To whom correspondence may be addressed. Email: jun.zhu@xmu.edu.cn or xiahp@sustech.edu.cn.

This article contains supporting information online at https://www.pnas.org/lookup/suppl/doi:10.1073/pnas.2215900120/-/DCSupplemental.

Published February 3, 2023.

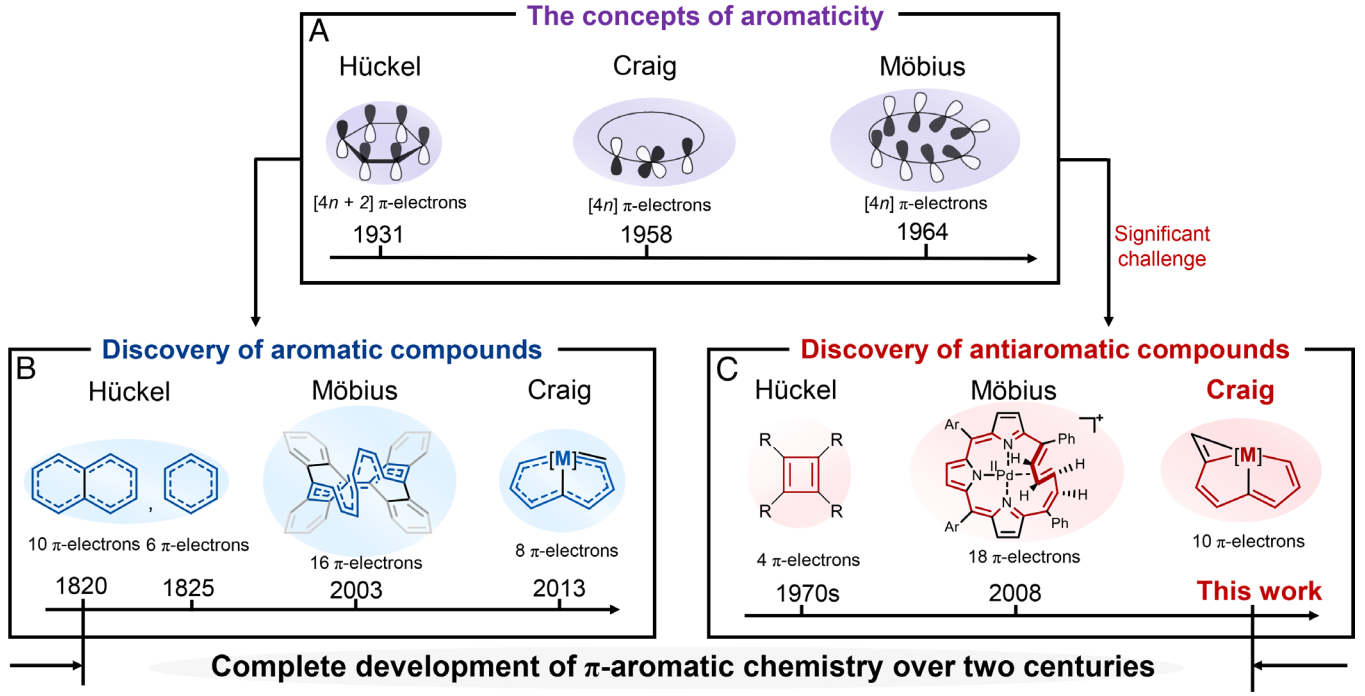

Fig. 1. Complete development of π-aromatic chemistry over the last two centuries. (*A*) The proposed concepts of aromaticity. (*B*) The discovery of aromatic molecules. (*C*) The discovery of antiaromatic molecules.

antiaromatic molecule is even more challenging. Although many efforts have been made to synthesize Craig antiaromatic molecules, the obtained compounds have ultimately adopted a nonplanar structure to alleviate the antiaromaticity destabilization. For example, Xi et al. reported in 2016 that dicupra[10]annulene (24) with the dihedral angle between two 1,3-diene planes is 77.8°. More recently, our group attempted to incorporate a bridgehead transition metal into naphthalene to convert a Hückel aromatic naphthalene into a Craig antiaromatic metal-bridgehead naphthalene (25), but a nonaromatic rather than an antiaromatic twisted geometry with a dihedral angle of 43.1° was ultimately obtained instead. Thus, the Craig antiaromatic compound has not been reported to date.

Herein, we developed a deprotonation-induced redox reaction-based strategy to synthesize the first planar Craig antiaromatic molecules, which are denoted complexes (**3**) (Fig. 2*A*). Single-crystal X-ray diffraction studies characterizing isolated complexes (**3**) revealed nearly perfectly planar fused five-member rings (5MRs) with significant alternation of the carbon–carbon bond lengths. The ^{1}H NMR spectra of complexes (**3**) showed remarkable upfield shifts of the proton peaks, which were similar to the NMR shifts computed for a classic antiaromatic heterocyclic five-membered ring (borole) (Fig. 2*E*). A combination of experimental and theoretical results demonstrates the Craig antiaromaticity of these compounds. We further synthesized a series of reactants with different acidity via substituting ligands and functional groups, and totally eight Craig antiaromatic compounds were obtained. It turns out that a higher acidity of reactants leads to the successful synthesis of these Craig antiaromatic compounds.

Results and Discussion

Synthesis and Characterization of Craig Antiaromatic Complexes (3). To prepare the Craig antiaromatic complexes (**3**), we synthesized complexes (**2**) (Fig. 2*A*) as start material, which is according to the previous predicted that acidity of a cyclic compound is expected to decrease by the antiaromaticity in its conjugated base (16). Complexes (**2**) were designed to contain two phosphonium groups, whose strongly electron-withdrawing character is expected to increase both the stability and the acidity of the reactant complexes (**2**) (16, 26), and the acidity of complexes (**2**) could be modulated by the different functional groups on cyclic structure and/or ligands on metal center. Mixing complex **1** (Fig. 2*A*) (27) with a propargyl phosphonium salt (28, 29) $[HC \equiv CCH_2PR_3]^+[BPh_4]^-$ containing different functional groups in dichloromethane (DCM) at room temperature (RT) produced complexes **2a** and **2b** (Fig. 2*A*). Ligand replacement reactions of **2a** and **2b** with CH_3CN (ACN) and 2,2′-bipyridine (bpy) at 60 °C led to formation of complexes **2a-ACN** and **2a-bpy**, **2b-ACN** and **2b-bpy**, respectively (Fig. 2*A*). Further investigation of the ^{31}P NMR spectra of these compounds showed two obvious signals for C*P*Ph_3, suggesting successful construction of two phosphonium groups in complexes (**2**) (Supplementary *SI Appendix*, Figs. S1, S6, S24, S29, S39 and S44). Complexes (**3**) were obtained by reacting complexes (**2**) with Et_2NH as a base, which was accompanied by a color change from brownish yellow to deep green (Fig. 2*A*). Specifically, mixing complex **2a** and **2b** with excess of Et_2NH and PPh_3 in DCM at RT afforded complexes **3a-PPh$_3$** and **3b-PPh$_3$**, respectively, in good yields (81% and 77% %, respectively). **3a-ACN**, **3a-bpy**, **3b-ACN,** and **3b-bpy** were synthesized by adding Et_2NH to their corresponding complexes (**2**) (Fig. 2*A*). To prepare complexes **3a-bpy** and **3b-bpy**, another method is through ligand replacement reactions of **3a-PPh$_3$** and **3b-PPh$_3$**, respectively, in the presence of bpy (Fig. 2*A*). However, **3a-ACN** and **3b-ACN** could not be synthesized from **3a-PPh$_3$** and **3b-PPh$_3$** by ACN ligand replacement because the PPh_3 ligand could not be substituted by the weak ACN ligand (Fig. 2*A*). In addition, the reactions converting complexes (**2**) to complexes (**3**) in the presence of a base (Et_2NH) could be reversed by adding an acid ($HCl{\cdot}Et_2O$ or $HBF_4{\cdot}Et_2O$) (Fig. 2*A*). As for stability,

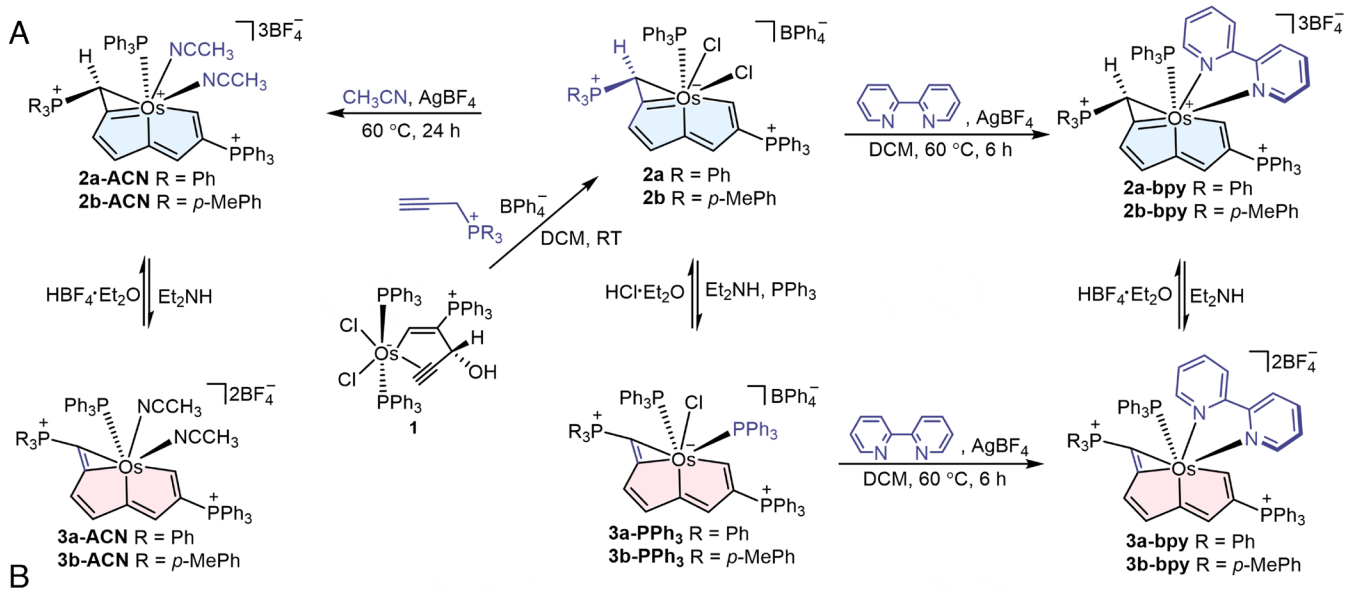

B

Bond length	Os1-C1	Os1-C4	Os1-C7	C1-C2	C2-C3	C3-C4	C4-C5	C5-C6	C6-C7
2a	2.003(9)	2.089(9)	1.969(8)	1.403(12)	1.393(12)	1.375(12)	1.405(12)	1.372(12)	1.386(12)
3a-PPh3	2.034(4)	2.102(4)	2.084(4)	1.344(6)	1.454(6)	1.347(6)	1.442(6)	1.346(6)	1.422(6)
2a-bpy	2.042(11)	2.073(10)	1.971(10)	1.392(14)	1.411(14)	1.381(14)	1.412(14)	1.391(14)	1.353(15)
3a-bpy	2.045(3)	2.095(4)	2.078(3)	1.364(5)	1.443(5)	1.352(5)	1.450(4)	1.344(5)	1.422(5)

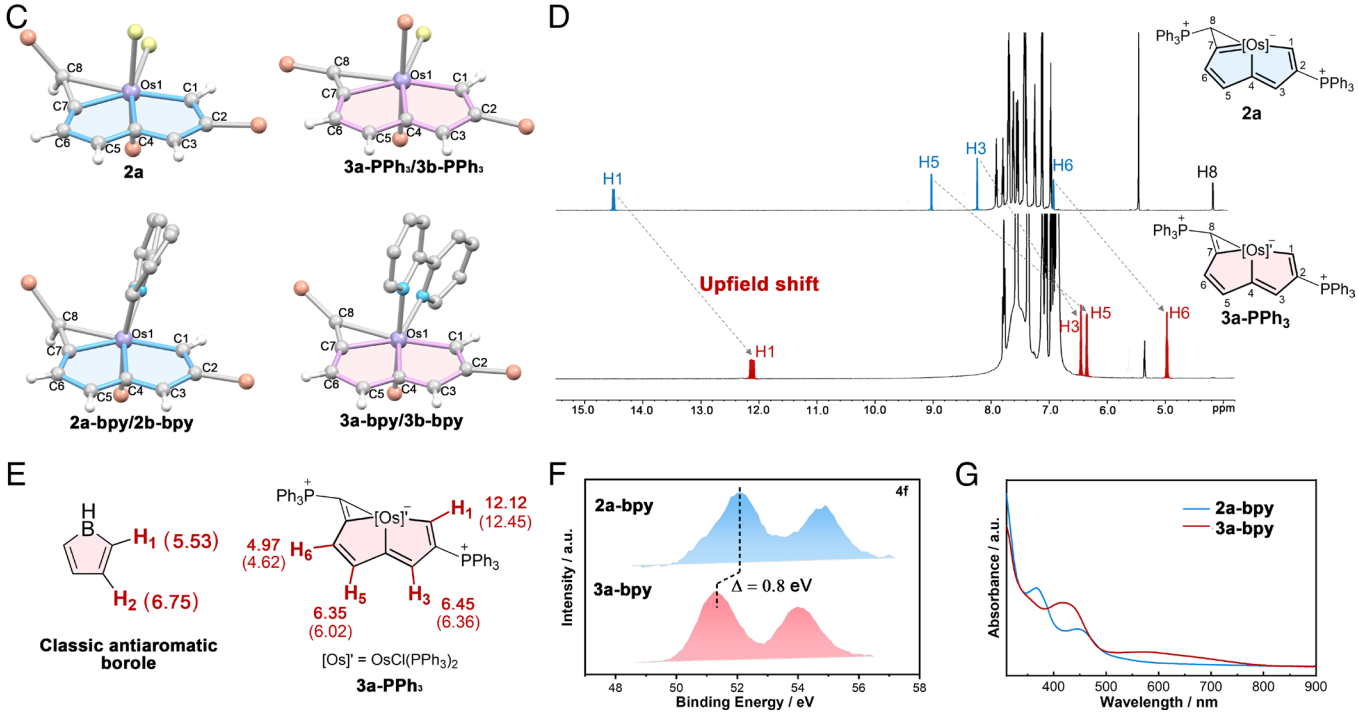

Fig. 2. (*A*) Synthesis of antiaromatic complexes (**3**) with different functional groups and ligands. (*B*) Labeling of the selected bond lengths in fused 5MRs for **2a**, **3a-PPh$_3$**, **2a-bpy**, and **3a-bpy**. Selected bond lengths are given in Å. (*C*) X-ray crystal structures for cations of **2a** and **3a-PPh$_3$**/**3b-PPh$_3$**, **2a-bpy**/**2b-bpy**, and **3a-bpy**/**3b-bpy** drawn with 50% probabilities (the phenyl groups, *p*-methylphenyl or cyclohexyl group in the PR$_3$ moieties are omitted for clarity). (*D*) Experimental ^{1}H NMR spectra showing an upfield shift in **3a-PPh$_3$** compared with **2a** in CD_2Cl_2. (*E*) Comparison of proton chemical shifts (theoretical values are in parenthesis) of **3a** to that of the classic antiaromatic borole with a heterocyclic 5MR (ppm versus tetramethylsilane). (*F*) Os 4f XPS spectra of complexes **2a-bpy** and **3a-bpy**. (*G*) UV–Vis–NIR absorption spectra of **2a-bpy** and **3a-bpy** (1.0×10^{-4} M) measured in CH_3CN at RT. Blue color represents aromatic species, whereas red color represents antiaromatic species.

complexes (**2**) were found to be more stable in air than complexes (**3**); solutions of the former in air were stable for several days, whereas solutions of the latter in air were decomposed completely in 2 h. Both complexes (**2**) and (**3**) were characterized by NMR and high-resolution mass spectrometry (HRMS) (*SI Appendix*, Figs. S1–S98).

Single-crystal X-ray diffraction was conducted to determine the structures of complexes (**2**) and (**3**) (Fig. 2 *B* and *C*). As shown in Fig. 2*C*, complexes (**2**) and (**3**), all have planar conjugated systems as reflected by the mean deviations from the least-squares plane of 0.028 Å (**2a**), 0.027 Å (**2a-bpy**), 0.016 Å (**2b-bpy**), 0.023 Å (**3a-PPh_3**), 0.023 Å (**3b-PPh_3**), 0.052 Å (**3a-bpy**) and 0.061 Å (**3a-bpy**) in the 5MRs (*SI Appendix*, Figs. S99–S106), respectively. Notably, the sum of the angles in 5MRs, such as 539.9(4)°/539.8(0)° in **2a** and 540.1(1)°/540.0(5)° in **3a-PPh_3** (*SI Appendix*, Figs. S99–S105), were all consistent with the ideal value 540° of the sum of the interior angles of a planar pentagon. Further comparison of these structures suggested that **3a-PPh_3** is similar to **2a** with a difference of only one proton in the C8 position of the conjugated framework, and this one proton difference was also observed between cationic **2a-bpy** and **3a-bpy** structures (Fig. 2*C*). However, significant differences in bond lengths were found in these otherwise similar frameworks (Fig. 2*B*). For example, the C–C bond lengths (C1–C7) in **3a-PPh_3** were 1.344(6), 1.454(6), 1.347(6), 1.442(6), 1.346(6) and 1.422(6) Å, but those of **2a** are 1.403(12), 1.393(12), 1.375(12), 1.405(12), 1.372(12) and 1.386(12) Å, demonstrating negligible bond alternation in **2a** but significant alternation in the bond lengths in **3a-PPh_3**, indicating the presence of alternating single and double C–C bonds in the latter (Fig. 2*B*). Likewise, similar negligible bond alternation was observed for **2a-bpy** and **2b-bpy**, and significant bond alternation was observed in **3b-PPh_3**, **3a-bpy** and **3b-bpy** (Fig. 2*B* and *SI Appendix*, Figs. S101–S105). This result was further verified by the analysis of the alternation of the C–C bonds in the 5MRs, and we first calculated the mean values of C–C bond such as 1.389 Å for complex **2a** and 1.392 Å for complex **3a-PPh_3**, which indicates their mean values of C–C bond is close. Then we calculated the SDs for the lengths of the six C–C bonds, as a very small SDs in complexes (**2**) (**2a**: 0.0127 Å, **2b**: 0.0174 Å, **2a-bpy**: 0.0199 Å and **2b-bpy**: 0.0156 Å), whereas much larger value in complexes (3) (**3a-PPh_3**: 0.0478 Å, **3b-PPh_3**: 0.0473 Å, **3a-bpy**: 0.0437 Å and **3b-bpy**: 0.0364 Å). In addition, the Os1-C7 bond lengths in complexes (3) (2.084 Å in **3a-PPh_3**, 2.087 Å in **3a-bpy**) were longer than those of in complexes (**2**) (1.969 Å in **2a**, 1.971 Å in **2a-bpy**), thus indicating the presence of formal Os-C single bonds in complexes (**3**). These results showed that complexes **2a**, **2a-bpy,** and **2b-bpy** have delocalized structures and are comparable to a Craig aromatic metallapentalene that was reported previously (30), whereas the planar complexes **3a-PPh_3**, **3b-PPh_3**, **3a-bpy,** and **3b-bpy** have localized structures with significant bond alternation, suggesting antiaromaticity.

^{1}H NMR spectra were obtained to investigate the antiaromaticity of the prepared compounds as the hydrogens outside the conjugated ring would be influenced by a shielding field and shift to upfield. Significant upfield shifts of the proton peaks in the spectrum of **3a-PPh_3** relative to those in the spectra of complexes **2a** were observed, even with the additional electron-withdrawing phosphonium group participating in the cyclic conjugated structure of the former complex (Fig. 2*D*). Specifically, the proton chemical signals of **3a-PPh_3** were upfield at 12.12, 6.45, 6.35, and 4.97 ppm, whereas those of **2a** were downfield at 14.49, 8.17, 8.96, and 6.83 ppm (Fig. 2*D* and *SI Appendix*, Table S1). Similarly, the ^{1}H NMR signals of all other complexes (**3**) were clearly upfield relative to those of the corresponding complexes (2), such as difference ranging from 2.11 to 3.40 ppm between **2a-ACN** and **3a-ACN** (*SI Appendix*, Table S1). Consistently, these distinctive upfield shifts of the proton peaks were also reproduced reasonably well by theoretical calculations (*SI Appendix*, Fig. S109). Furthermore, the ^{1}H NMR signals corresponding to H3, H5 and H6 in the spectrum of **3a-PPh_3** (Fig. 2*E*) were at 6.45, 6.35, and 4.97 ppm, respectively, which are within the range reported for antiaromatic peripheral hydrogens (31, 32). In addition, the ^{1}H NMR signals corresponding to H3, H5, and H6 in the spectrum of **3a-PPh_3** were similar to the proton chemical shifts calculated for the antiaromatic borole (H1: 5.53 and H2: 6.75 ppm, Fig. 2*E*). The ^{1}H NMR signal corresponding to H1 in the spectrum of **3a-PPh_3** was downfield than those of H3, H5, and H6 because of the proximity of this proton to both the transition metal and the electron-withdrawing phosphonium group (33), but this signal was still shifted upfield by 2.37 ppm with respect to the H1 peak in the spectrum of **2a** (Fig. 2 *D* and *E*). The significant upfield shifts of proton peaks to the antiaromatic peripheral hydrogens indicate the antiaromaticity of the complexes (**3**).

As Craig aromaticity involves the electrons from *d* orbital for $p\pi$–$d\pi$ interactions in a π-conjugated system, the prepared complexes were further investigated by X-ray photoelectron spectroscopy (XPS), from which the changes in the valence state of the osmium center reflected by binding energy were applied to correlate the change in the number of electrons in the *d* orbital. The binding energies of these complexes were determined, with a lower binding energy corresponding to a lower valence state with more electrons in the *d* orbital (34). As shown in Fig. 2*F*, the binding energies of osmium in **3a-bpy** were clearly much lower than that in **2a-bpy**. All binding energies are referenced to a C 1s value of 285.0 eV (34). The difference in the Os $4f_{7/2}$ binding energies of **2a-bpy** (52.1 eV) and **3a-bpy** (51.3 eV) was 0.8 eV, and the same difference was found between **2a** (51.9 eV) and **3a-PPh_3** (51.1 eV) (Fig. 2*F* and *SI Appendix*, Fig. S107). All of these results indicated that the valence states of osmium in complexes **3a-bpy** and **3a-PPh_3** were lower than those in complexes **2a-bpy** and **2a**, respectively, which is in line with the formal valence state of complexes (**2**) (+6) and (**3**) (+4). These significant differences were attributed to a remarkable change in the number of electrons in *d* orbitals, clearly indicating that the conversion from complexes (**2**) to (**3**) is a deprotonation-induced reduction process. Note that the number of electrons in the *d* orbital between complexes (**2**) and (**3**) is different, which might be connected to the opposite number of π-conjugated electron between Craig aromaticity and antiaromaticity. Thus, this difference might lead to the change of the number of electrons from *d* orbital in p_π–d_π interactions, enabling the Craig antiaromaticity in complexes (**3**). In addition, UV–Vis–NIR absorption spectra of these complexes were obtained, and the spectra of both **3a-bpy** and **3a-PPh_3** exhibited weak absorption with redshifted bands at 573 and 607 nm in comparison with those of **2a-bpy** (λ_{max} = 444 nm) and **2a** (λ_{max} = 461 nm), respectively, which is consistent with the previous work reported that the antiaromatic molecule would exhibit a weak long tail with redshift character (32) (Fig. 2*G* and *SI Appendix*, Fig. S108). Overall, our experimental observations all pointed the Craig antiaromaticity in the complexes (**3**).

Theoretical Study of Craig Antiaromaticity Properties of Prepared Complexes (3). To further examine the antiaromaticity of complexes (3), we followed by conducting the density-functional theory (DFT) calculations. We began with the optimized geometries of complexes (3), which consisted of planar structures with significant bond alternation in localized 5MRs, whereas optimized geometries of complexes (**2**) exhibited negligible bond alternation and delocalized structures, consistent with the experimental observations (*SI Appendix*, Fig. S110). Moreover, simplified models for complexes **3′**, **3-ACN′** and **3-bpy′**, with relatively small **PMe_3** ligands and hydrogen atoms in place of the **PPh_3** ligands and phosphonium substituents, respectively, showed similar bond alternation in the bond lengths and planar structure 5MR structures (*SI Appendix*, Table S5). The results

of all geometries of complexes optimized are in line with our experimental observations, showing the reliability of theoretical calculation and could be applied to the following (anti)aromaticity calculations.

We performed canonical molecular orbital (CMO) nucleus-independent chemical shift (NICS) calculations on the simplified models to gain further insight into the antiaromaticity of prepared complexes (35, 36). The NICS(0)$_{zz}$ describes the zz component above the geometrical center, and the NICS(0)π_{zz} has been shown to be a suitable indicator of π-aromaticity (36), whereas NICS(0)$_{\sigma}$ is suitable for assessing σ-aromaticity (37), with negative values generally indicating aromaticity and positive values indicating antiaromaticity. As shown in Fig. 3*A*, the NICS(0)π_{zz} values for the 5MRs of **3′**, denoted ring **L** and ring **R**, were +28.4 and +28.6 ppm, respectively. Positive NICS(0)π_{zz} values were also found for **3-ACN′** (+27.2 ppm in **L** and +24.4 ppm in **R**) and **3-bpy′** (+35.1 ppm in **L** and +36.5 ppm in **R**) (Fig. 3*E* and *SI Appendix*, Fig. S111), which indicates that the ligands on the osmium center had minor effects on the antiaromaticity of the 5MR conjugated system. In addition, the negative NICS(0)$_{\sigma}$ values calculated in 3MR of **3′**, **3-bpy′,** and **3-ACN′** (−37.2, −48.5, and −36.9 ppm) suggest σ-aromaticity in 3MR, similar to the previous report (37). Similar calculations were also performed for the classic aromatic benzene (**4′**) and antiaromatic borole (**5′**) structures (Fig. 3*A* and *SI Appendix*, Fig. S112) for comparison. The NICS(0)π_{zz} value of benzene was −35.7 ppm, whereas that for borole was +43.2 ppm (Fig. 3*A*), consistent with the aromaticity and antiaromaticity, respectively, of these structures. The highly positive NICS(0)π_{zz} values of **3′**, **3-ACN′,** and **3-bpy′** were all consistent with that of the antiaromatic borole, but were in sharp contrast to that of aromatic benzene, verifying the antiaromaticity of **3′**, **3-ACN′,** and **3-bpy′**.

The antiaromaticity of **3′** was also investigated by anisotropy of the current induced density (ACID) calculation (38). The ACID function is obtained by adding products of the tensor elements of the current density susceptibility function. In general, diatropic

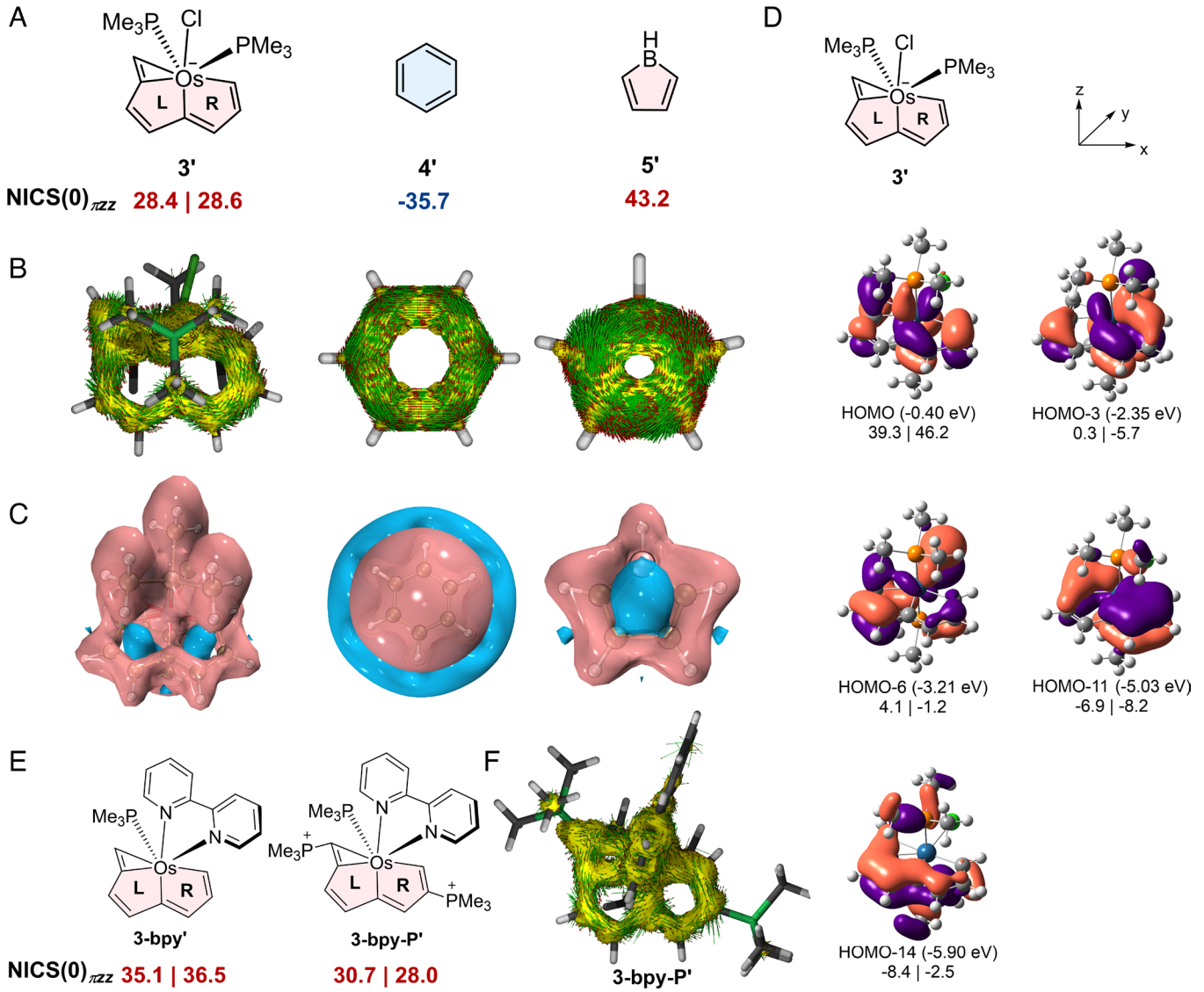

Fig. 3. (*A*) NICS(0)π_{zz} values (in ppm) for **3′, 4′,** and **5′**. (*B*) Computed ACID plots of **3′, 4′,** and **5′** from the π contributions, displayed with an isosurface value of 0.03 a.u. (*C*) ICSS$_{zz}$ plot of **3′, 4′,** and **5′**, the red surface indicates shielding, whereas the blue surface indicates deshielding. (*D*) Key occupied π MOs and their energies together with eigenvalues in parentheses for **3′**. (*E*) Comparison between NICS(0)π_{zz} values (in ppm) of **3-bpy′** and **3-bpy-P′** to investigate the impact of phosphonium substituents on the Craig antiaromaticity. (*F*) ACID plots of **3-bpy-P′** computed from the π contribution are displayed with an isosurface value of 0.02 a.u.

ring current indicates aromaticity, whereas paratropic ring current exhibits antiaromaticity. The distinct counterclockwise paratropic circulation in the π-system of **3′** indicated that antiaromaticity is similar to that exhibited by borole **5′** and stood in sharp contrast to the clockwise ring current of benzene **4′** (Fig. 3*B* and *SI Appendix*, Figs. S113–S115). Similar counterclockwise paratropic circulation was also found for **3-ACN′** and **3-bpy′** (*SI Appendix*, Figs. S116 and S117). Analysis of the iso-chemical shielding surface (ICSS) (39) was also performed to investigate the antiaromaticity of **3′**. As shown in Fig. 3*C*, the zz component of ICSS ($ICSS_{zz}$) in **3′** was plotted with a deshielding cone (blue) surrounded by a shielding loop (red) and was similar to the $ICSS_{zz}$ of the antiaromatic borole **5′**. Likewise, a deshielding cone surrounded by a shielding loop was also observed for **3-ACN′** and **3-bpy′** (*SI Appendix*, Fig. S118). In contrast, a shielding cone surrounded by a deshielding loop was found in the $ICSS_{zz}$ of benzene **4′** (Fig. 3*C*). Both the paratropic ring current of ACID and shielding loop surrounding of $ICSS_{zz}$ results verify the antiaromaticity in **3′**, **3-ACN′** and **3-bpy′**, in line with the NICS(0)π_{zz} values. Furthermore, isomerization stabilization energy (ISE) (40) and electron density of delocalized bonds (EDDB) (41) calculations were performed, respectively. As shown in *SI Appendix*, Figs. S119 and S120, the positive ISE values and the significantly reduced EDDB values both support the antiaromaticity in 5MRs.

To probe the origin of the antiaromaticity in **3′**, the electronic structure of these complexes was investigated. As shown in Fig. 3*D*, five occupied π molecular orbitals (π-MOs) of **3′**, namely the HOMO, HOMO-3, HOMO-6, HOMO-11, and HOMO-14, formed an eight-center 10-electron (8c-10e) antiaromatic system. Of these occupied orbitals, HOMO, HOMO-3, and HOMO-11 participated in $p\pi - d\pi$ interaction in the π-MOs involved the phase shift in the osmium center. These results showed that **3′** consists of the properties of $[4n + 2]$ π electrons, $p\pi$–$d\pi$ interaction and planarity, demonstrating **3′** exhibits Craig antiaromaticity. Similarly, five occupied π-MOs forming 8c-10e Craig antiaromatic systems were also found for **3-ACN′** and **3-bpy′** (*SI Appendix*, Fig. S111). Similar calculations were conducted for benzene and borole. We found three occupied π-MOs forming a 6c-6e Hückel aromatic system in benzene **4′** and two occupied π-MOs forming a 5c-4e Hückel antiaromatic system in borole **5′**, demonstrating the reliability of the calculations (*SI Appendix*, Fig. S112). All these results suggested that **3′**, **3-ACN′** and **3-bpy′** exhibit Craig antiaromaticity.

In addition, **3-bpy-P′** model was further calculated to investigate the impact of the phosphonium substituent on aromaticity (Fig. 3*E* and *SI Appendix*, Fig. S121). As shown in Fig. 3*E*, the NICS(0)π_{zz} values of **3-bpy-P′** were +30.7 ppm for **L** ring and +28.0 ppm for **R** ring. Although the NICS(0)π_{zz} values of **3-bpy-P′** were slightly lower than those of the simplified model of **3-bpy′** (+35.1 ppm in **L** ring and +36.5 ppm in **R** ring), the highly positive values still indicated the antiaromaticity of **3-bpy-P′**. In addition, analysis of the electronic structures of **3-bpy-P′** suggests an 8c-10e Craig antiaromatic character (*SI Appendix*, Fig. S121). An anticlockwise ring current in the ACID plots of **3-bpy-P′** was observed (Fig. 3*F* and *SI Appendix*, Fig. S122). All these results demonstrated that **3-bpy-P′** is similar to **3-bpy′** and exhibits Craig antiaromaticity.

Driving Force for the Synthesis of Craig Antiaromatic Compounds. Once the Craig antiaromaticity of complexes (**3**) had been clearly established both experimentally and theoretically, the next aim was to determine the driving force in the realization of Craig antiaromatic compounds via this deprotonation-induced reduction process. A series of complexes (**2**) with different acidity of H8 were synthesized (Fig. 4). By comparison with the synthesis in Fig. 2*A*, we found that the method used to form **3a-PPh$_3$** and **3b-PPh$_3$** from **2a** and **2b** failed to generate **3c-PPh$_3$** from **2c** (Fig. 4*A* and *SI Appendix*, Figs. S11–S15 and S86). As the only structure difference among **2a**, **2b,** and **2c** is the phosphonium group, we assumed that the failure of **3c-PPh$_3$** is possibly because the acidity of H8 of reactant **2c** was decreased with weaker electron-withdrawing nature of the tricyclohexyl phosphonium group by comparing with **2a** and **2b**. To test this hypothesis, monocationic complexes (**2**) [e.g., **2d-PPh$_3$**(30)] (Fig. 4*B* and *SI Appendix*, Fig. S123*A*) with lower acidity and tricationic complexes **2c-ACN** and **2c-bpy** (Fig. 4*C*) with higher acidity were synthesized

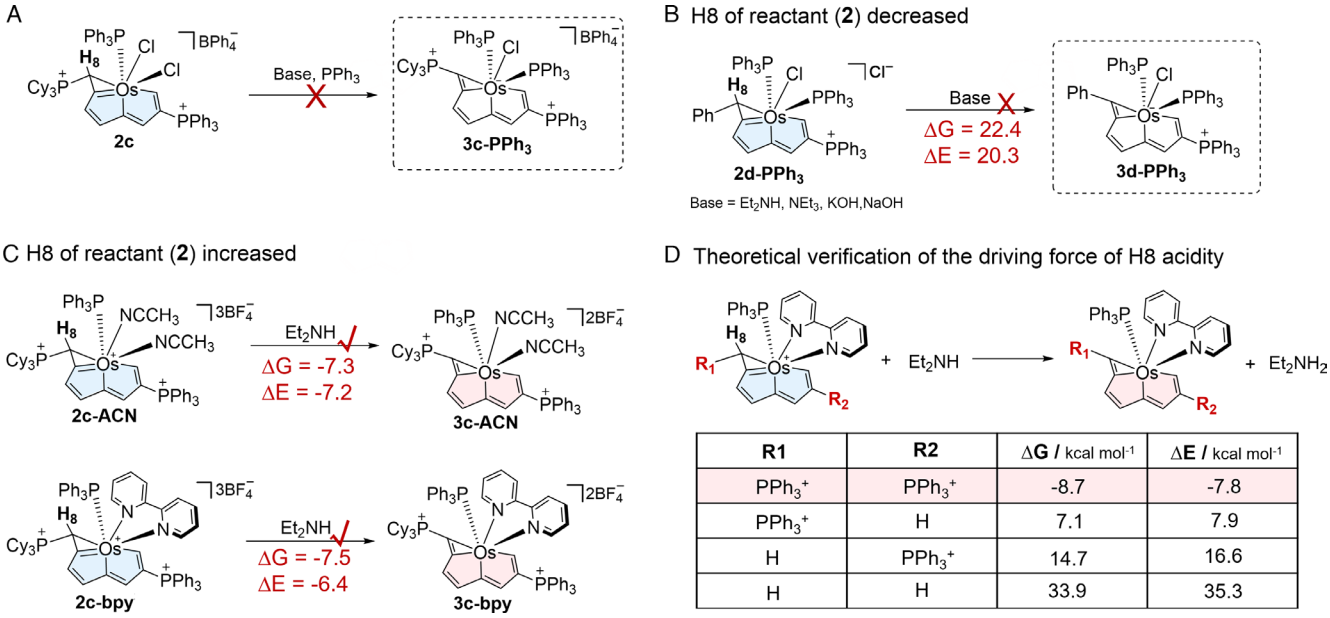

R1	R2	ΔG / kcal mol^{-1}	ΔE / kcal mol^{-1}
PPh_3^+	PPh_3^+	-8.7	-7.8
PPh_3^+	H	7.1	7.9
H	PPh_3^+	14.7	16.6
H	H	33.9	35.3

Fig. 4. (*A*) Experimental failure of forming **3c-PPh$_3$** from **2c**. Experimental verification by decreasing (*B*) and increasing (*C*) acidity of H8 in a series of reactants (**2**), along with theoretical calculations of free Gibbs energies at 298 K and electronic energies (kcal mol^{-1}) with Et_2NH as a base. (*D*) Theoretical verification of the driving force of H8 acidity.

(*SI Appendix*, Method). As we can see, monocationic complexes **2d-PPh$_3$** were not deprotonated by a base (e.g., Et_2NH, NEt_3, and NaOH) and exhibited thermodynamically unfavorable energies of 22.4 kcal mol^{-1} in forming **3d-PPh$_3$** (Fig. 4*B*). However, the tricationic complexes **2c-ACN** and **2c-bpy** readily react with Et_2NH to generate **3c-ACN** and **3c-bpy** (ΔG = –7.3 and –7.5 kcal mol^{-1}, respectively, as shown in Fig. 4). The hypothesis regarding the acidity of H8 among complexes (**2**) was supported by pKa calculations (42), as shown in *SI Appendix*, Fig. S123*B*. Specifically, the pKa values gradually decreased from monocationic **2d-PPh$_3$** to tricationic **2c-ACN**, which indicated that the acidity of these complexes was enhanced. In addition, this hypothesis was supported by further calculations of additional models (Fig. 4*D*) in which the highly electron-withdrawing phosphonium groups were gradually replaced with hydrogen, thus decreasing the acidity. The reactions changed from exergonic (–8.7 kcal mol^{-1} with two phosphonium groups) to endergonic (7.1 or 14.7 kcal/mol^{-1} with phosphonium and hydrogen, and 33.9 kcal mol^{-1} with two hydrogens). These results all suggested that the formation of antiaromatic (**3**) is determined by the acidity of H8 in complexes (**2**). Note that the reaction of (**2**) → (**3**) is an acid-base neutralization process, which is highly exergonic, and a higher acidity of (**2**) favors the synthesis of Craig antiaromatic species (**3**). Therefore, the driving force for the realization of Craig antiaromatic compounds was determined to be the energy released by acid-base neutralization.

Conclusion

We have developed a strategy to synthesize, isolate, and characterize a planar Craig antiaromatic species (**3**) for the first time; the synthesis was based on a deprotonation-induced reduction process, and the antiaromaticity of the obtained molecules was evidenced by both experimental characterizations and theoretical calculations. Further experiments along with thermodynamic analysis supported by pKa and relevant reaction energy profile calculations revealed that the intrinsic driving force for realization of Craig antiaromatic compounds is the highly exothermic acid-base chemistry. This work supports the realization of the first Craig antiaromatic species, 203 y after the discovery of the aromatic compound naphthalene and completes a full picture of π-aromatic chemistry. The discovery of Craig antiaromatic molecules with $[4n + 2]$ π electrons could encourage further development of such a unique antiaromatic system and significantly enrich the chemistry of aromaticity.

Materials and Methods

All syntheses were carried out under an inert atmosphere (nitrogen or argon) using standard Schlenk techniques unless otherwise stated. Solvents were distilled under nitrogen from sodium/benzophenone (hexane and diethyl ether) or calcium hydride (DCM) prior to use. The starting materials $[OsCl_2(CHC(PPh_3)CH(OH) \equiv CH)(PPh_3)_2]$ (1) (24) and the propargyl phosphonium salt (25, 26) $[HC \equiv CCH_2PR_3]^+[BPh_4]^-$ (R = Ph, Cy, *p*-MePh) were prepared as described in the cited references. And other reagents were used as received from commercial sources without further purification. All the optimizations were performed with the Gaussian 09 software package at 298 K. The CMO NICS calculations were carried out with the NBO 7.0 program and Gaussian 16 software package at 298 K. The ACID calculations were carried out with the ACID program. The ICSSs analysis calculations were carried out with Multiwfn and visualized by the VMD program. For computational details, see *SI Appendix*.

Data, Materials, and Software Availability. All study data are included in the article and/or *SI Appendix*. Crystallographic data have been deposited in the Cambridge Crystallographic Data Centre (CCDC) under accession numbers CCDC: 1550304 (**2a**), 1527078 (**3a-PPh$_3$**), 1527079 (**2a-bpy**), 1527080 (**3a-bpy**), 2127863 (**3b-bpy**), 2124386 (**3b-PPh$_3$**), 2130871 (**2b-bpy**) and 2130872 (**2c**). These data can be obtained free of charge from the Cambridge Crystallographic Date Centre via https://www.ccdc.cam.ac.uk/data_request/cif.

ACKNOWLEDGMENTS. This work is supported by the National Natural Science Foundation of China (Nos. 92156021, 21873079, and 21931002), the Shenzhen Science and Technology Innovation Committee (no. JCYJ20200109140812302), the Guangdong Provincial Key Laboratory of Catalysis (no. 2020B121201002), The UK EPSRC (EP/W03784X/1), the Top-Notch Young Talents Program of China, and the Financial Support for Outstanding Talents Training Fund in Shenzhen.

Author affiliations: [a]State Key Laboratory of Physical Chemistry of Solid Surfaces, Collaborative Innovation Center of Chemistry for Energy Materials, College of Chemistry and Chemical Engineering, Xiamen University, Xiamen 361005, China; [b]Fujian Provincial Key Laboratory of Theoretical and Computational Chemistry, College of Chemistry and Chemical Engineering, Xiamen University, Xiamen 361005, China; [c]Shenzhen Grubbs Institute and Department of Chemistry, Southern University of Science and Technology, Shenzhen 518005, China; and [d]Department of Chemical Engineering, Loughborough University, Loughborough, Leicestershire LE11 3TU, United Kingdom

1. E. Hückel, Quantum-theoretical contributions to the benzene problem. *Z. Phys.* **70**, 204–286 (1931).
2. D. Craig, N. L. Paddock, A novel type of aromaticity. *Nature* **181**, 1052–1053 (1958).
3. E. Heilbronner, Hückel molecular orbitals of Möbius-type conformations of annulenes. *Tetrahedron Lett.* **5**, 1923–1928 (1964).
4. D. Ajami, O. Oeckler, A. Simon, R. Herges, Synthesis of a Möbius aromatic hydrocarbon. *Nature* **426**, 819–821 (2003).
5. M. Saito *et al.*, Dilithioplumbole: A lead-bearing aromatic cyclopentadienyl analog. *Science* **328**, 339–342 (2010).
6. L. F. Cheung, G. S. Kocheril, J. Czekner, L.-S. Wang, Observation of Möbius aromatic planar metallaborocycles. *J. Am. Chem. Soc.* **142**, 3356–3360 (2020).
7. J. K. Pagano *et al.*, Actinide 2-metallabiphenylenes that satisfy Hückel's rule. *Nature* **578**, 563–567 (2020).
8. Y. Zhang *et al.*, Metalla-aromatics: Planar, nonplanar, and spiro. *Acc. Chem. Res.* **54**, 2323–2333 (2021).
9. B. J. Frogley, L. J. Wright, Recent advances in metallaaromatic chemistry. *Chem. Eur. J.* **24**, 2025–2038 (2018).
10. D. W. Szczepanik, M. Solà, Electron delocalization in planar metallacycles: Hückel or möbius aromatic? *ChemistryOpen* **8**, 219–227 (2019).
11. M. Mauksch, S. B. Tsogoeva, Demonstration of "Möbius" aromaticity in planar metallacycles. *Chem. Eur. J.* **16**, 7843–7851 (2010).
12. Z. Huang *et al.*, A tris-spiro metalla-aromatic system featuring Craig-Möbius aromaticity. *Nat. Commun.* **12**, 1319 (2021).
13. J. Kidd, W. H. Wollaston, XVI. Observations on naphthaline, a peculiar substance resembling a concrete essential oil, which is apparently produced during the decomposition of coal tar, by exposure to a red heat. *Phil. Trans. R. Soc. London* **111**, 209–221 (1821).
14. M. Faraday, XX. On new compounds of carbon and hydrogen, and on certain other products obtained during the decomposition of oil by heat. *Phil. Trans. R. Soc. London* **115**, 440–466 (1825).
15. C. Zhu *et al.*, Stabilization of anti-aromatic and strained five-membered rings with a transition metal. *Nat. Chem.* **5**, 698–703 (2013).
16. R. Breslow, Antiaromaticity. *Acc. Chem. Res.* **6**, 393–398 (1973).
17. D. Y. Zubarev, B. B. Averkiev, H.-J. Zhai, L.-S. Wang, A. I. Boldyrev, Aromaticity and antiaromaticity in transition-metal systems. *Phys. Chem. Chem. Phys.* **10**, 257–267 (2008).
18. H. Kimling, A. Krebs, Synthesis of a cyclobutadiene stabilized by steric effects. *Angew. Chem. Int. Ed.* **11**, 932–933 (1972).
19. G. Mayer, S. Pfriem, U. Schäfer, R. Matusch, Tetra-tert-butyltetrahedran. *Angew. Chem. Int. Ed.* **90**, 552–553 (1978).
20. H. Irngartinger, N. Riegler, K.-D. Malsch, K.-A. Schneider, G. Maier, Structure of tetra-tert-butylcyclobutadiene. *Angew. Chem. Int. Ed.* **19**, 211–212 (1980).
21. A. Deniz Ashok, S. Peters Kevin, J. Snyder Gary, Experimental determination of the antiaromaticity of cyclobutadiene. *Science* **286**, 1119–1122 (1999).
22. E. Pacholska-Dudziak *et al.*, Palladium vacataporphyrin reveals conformational rearrangements involving Hückel and Möbius macrocyclic topologies. *J. Am. Chem. Soc.* **130**, 6182–6195 (2008).
23. V. Minkin, M. Glukhovstev, B. Simkin, *Aromaticity and Antiaromaticity: Electronic and Structural Aspects* (Wiley, 1994).
24. J. Wei *et al.*, Aromatic dicupra [10] annulenes. *J. Am. Chem. Soc.* **138**, 60–63 (2016).
25. C. Tang *et al.*, Releasing antiaromaticity in metal-bridgehead naphthalene. *J. Am. Chem. Soc.* **143**, 15587–15592 (2021).
26. S. Chen *et al.*, Addition of alkynes and osmium carbynes towards functionalized d_π–p_π conjugated systems. *Nat. Commun.* **11**, 4651 (2020).
27. H. Xia *et al.*, Osmabenzenes from the reactions of HC≡CCH(OH)C≡CH with $OsX_2(PPh_3)_3$ (X= Cl, Br). *J. Am. Chem. Soc.* **126**, 6862–6863 (2004).
28. A. L. Colebatch, I. A. Cade, A. F. Hill, M. M. Bhadbhade, η2-Allenyl-and η2-alkynylphosphonium complexes of platinum. *Organometallics* **32**, 4766–4774 (2013).
29. G. B. Bagdasaryan, P. S. Pogosyan, G. A. Panosyan, M. G. Indzhikyan, Synthesis and transformations of triphenylpropargylphosphonium bromide. *Russ. J. Gen. Chem.* **78**, 1177–1183 (2008).

30. C. Zhu *et al.*, σ-Aromaticity in an unsaturated ring: Osmapentalene derivatives containing a metallacyclopropene unit. *Angew. Chem. Int. Ed.* **54**, 3102–3106 (2015).
31. J. Cao *et al.*, The impact of antiaromatic subunits in [4 n + 2] π-systems: Bispentalenes with [4 n + 2] π-electron perimeters and antiaromatic character. *J. Am. Chem. Soc.* **137**, 7178–7188 (2015).
32. T. Xu *et al.*, Antiaromatic dicyclopenta[b, g]/[a, f]naphthalene isomers showing an open-shell singlet ground state with tunable diradical character. *J. Am. Chem. Soc.* **143**, 20562–20568 (2021).
33. J. Chen, G. Jia, Recent development in the chemistry of transition metal-containing metallabenzenes and metallabenzynes. *Coord. Chem. Rev.* **257**, 2491–2521 (2013).
34. D. Salmon, R. Walton, Reactions of osmium tetraoxide with triphenylphosphine. Reformulation of oxotrichlorobis (triphenylphosphine) osmium (V). *Inorg. Chem.* **17**, 2379–2382 (1978).
35. Z. Chen, C. S. Wannere, C. Corminboeuf, R. Puchta, P. v. R. Schleyer, Nucleus-independent chemical shifts (NICS) as an aromaticity criterion. *Chem. Rev.* **105**, 3842–3888 (2005).
36. H. Fallah-Bagher-Shaidaei, C. S. Wannere, C. Corminboeuf, R. Puchta, P. v. R. Schleyer, Which NICS aromaticity index for planar π rings is best? *Org. Lett.* **8**, 863–866 (2006).
37. J. Wu *et al.*, σ-Aromaticity in a fully unsaturated ring. *Asian J. Chem.* **13**, 3691–3696 (2018).
38. D. Geuenich, K. Hess, F. Köhler, R. Herges, Anisotropy of the induced current density (ACID), a general method to quantify and visualize electronic delocalization. *Chem. Rev.* **105**, 3758–3772 (2005).
39. S. Klod, E. Kleinpeter, Ab initio calculation of the anisotropy effect of multiple bonds and the ring current effect of arenes–application in conformational and configurational analysis. *J. Chem. Soc. Perkin Trans.* **2**, 1893–1898 (2001).
40. C. S. Wannere *et al.*, On the stability of large [4n]annulenes. *Org. Lett.* **5**, 2983–2986 (2003).
41. D. W. Szczepanik *et al.*, A uniform approach to the description of multicenter bonding. *Phys. Chem. Chem. Phys.* **16**, 20514–20523 (2014).
42. S. R. Neufeldt, G. Jiménez-Osés, J. R. Huckins, O. R. Thiel, K. N. Houk, Pyridine N-oxide vs pyridine substrates for Rh(III)-catalyzed oxidative C-H bond functionalization. *J. Am. Chem. Soc.* **137**, 9843–9854 (2015).